JOURNAL OF MATERIALS SCIENCE 30 (1995) 2911–2920

# Direct production of ultrafine amorphous Fe–P alloy particles by the plasma method

S. M. HUANG*, X. H. YU, C. Z. YANG
*Chemistry Department of Nanjing University, Nanjing 210008, People's Republic of China*

Ultrafine amorphous Fe–P alloy particles were directly synthesized by the plasma using cyclopentenyl iron and phosphorous trichloride as starting materials. The plasma gas greatly influenced the morphology, dispersion and composition.The particles were roughly spherical with a diameter of 40–200 nm and had the composition of $Fe_{106}P_{50}$. Elemental chlorine was found in the surface of the particle especially prepared under argon plasma conditions. It was bonded with phosphorus and carbon in Fe–P particles prepared in argon plasma and mainly with carbon in Fe–P particles deposited under a hydrogen plasma. Formation of Fe–P improves the stability of phosphorus in air. Phosphorus enrichment in the surface of Fe–P particles was also found. The particles were characterized by TEM, SEM, infrared-spectroscopy, X-ray photoelectron spectroscopy quantitative analysis, differential scanning colorimetry, inductively coupled plasma, X-ray diffraction and X-ray microprobe analysis. The formation mechanism of Fe–P amorphous particles was also discussed.

## 1. Introduction

In recent years, amorphous alloy has received considerable attention owing to its expected applications in magnetic recording, ferroiluids, catalysis and radar-absorption materials (RAM) [1–4]. A number of techniques such as rapid solidification, electroless deposition, electrodeposition, sputter deposition, ion implantation, laser glazing, chemical vapour deposition, solid-state reaction and chemical reduction have been developed for the preparation of this kind of material [5–15]. In chemical vapour deposition (CVD), the plasma technique is a powerful tool to produce ultrafine powders of ceramics and refractory metals. Many plasma chemical vapour deposition processes have been studied to synthesize ultrafine ceramics powders such as SiC, SiN, SiB, WC, TiC, $Si_3N_4$, AlN and metals such as titanium, molybdenum, tungsten, etc. and also metal particles dispersed in polymer using r.f. plasma [16–18] and d.c. plasma [19–21]. However, little work has focused on the synthesis of Fe–P ultrafine amorphous alloy powder by the plasma technique. In this paper, the direct production of ultrafine amorphous Fe–P alloy powder by plasma method is reported. The synthesis process and the properties of the ultrafine amorphous powders were studied.

## 2. Experimental procedure

### 2.1. Materials

$Fe(CP)_2$ was obtained from Shanghai Chem. Agent Co. and purified by sublimation before use. $PCl_3$ was C.P. grade. Argon and hydrogen gas were used as plasma gas without further purification before use.

### 2.2. Plasma apparatus and experimental process

The plasma apparatus was equipped with a radio frequency (r.f., 13.56 MHz) power generator, which can create an inductively coupled electrodeless glow discharge. A glass tubular reactor, 8 cm diameter and 30 cm long, was evacuated from the right side using a cold trap and a rotary vacuum pump. The pressure in the system was monitored by a vacuum gauge. Solid $Fe(CP)_2$was heated by a water bath. Two glass plates (length 15 cm) within the reactor were overlaid with a number of copper grids coated with carbon film and a number of glass grids at positions A and B as shown in Fig. 1. The copper grids were used for direct TEM and SEM observation and the glass grids were used for X-ray photoelectron spectroscopy (XPS) measurement. The system was first evacuated by the rotary vacuum pump until a pressure of $10^{-3}$ torr was achieved. Argon gas containing $PCl_3$ was then introduced into the reactor to displace the residual gases. Evacuation and argon introduction were repeated several times. The system was then again evacuated to $10^{-3}$ torr (1 torr = 133.322 Pa). Then the $Fe(Cp)_2$ was heated and the argon gas containing $PCl_3$ was also bled into the reactor. Finally, the pressure was controlled at 0.3–0.5 torr by appropriate opening of the argon or hydrogen gas inlet value. Imposition of 35 W r.f. power, 150 mA, created the conditions, under

* To whom all correspondence should be addressed.

0022–2461 © *1995 Chapman & Hall*

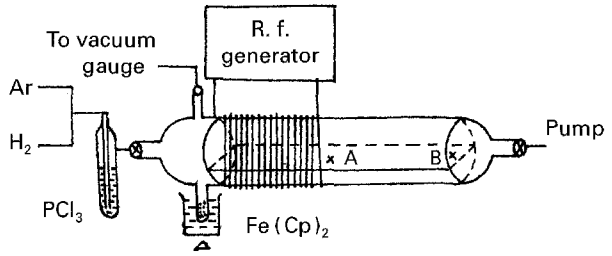


*Figure 1* The experimental apparatus.

TABLE I The experimental conditions used

| Sample | Original material | Plasma gas | Deposition time (min) | Total pressure (torr) |
|---|---|---|---|---|
| PL1 | $Fe(CP)_2$ | Ar | 20 | 0.3 |
| PL2a | $PCl_3$ | Ar | 20 | 0.3 |
| PL2b | $PCl_3$ | $H_2$ | 20 | 0.3 |
| PL3 | $Fe(CP)_2 + PCl_3$ | Ar | 40 | 0.5 |
| PL4 | $Fe(CP)_2 + PCl_3$ | $H_2$ | 40 | 0.5 |

which the synthesis of iron, phosphorus and Fe–P alloy particles was carried out. The process lasted for 20–40 min. Then the reactor was kept under vacuum until the XPS measurement was performed. The apparatus is shown in Fig. 1. The experimental conditions are listed in Table I.

### 2.3. Fourier transform–infrared (FT–IR) spectroscopy

Samples for IR spectroscopy were scraped from slides using a knife, and were incorporated into KBr disks. The IR spectra were obtained on a Nicolet 170 SX FT–IR spectrometer.

### 2.4. XPS measurement

The sample was exposed to air for less than 5 min while transferring it from the reactor into the XPS spectrometer. The XPS spectra were obtained using a M8200 XPS spectrometer with an Mg*K* X-ray source at 10 kV and 400 W at $10^{-8}$ torr. All peaks were referenced to the $C_{1s}$ peak at 284.60 eV. Spectra were reproducible to $\pm 0.1$ eV. Satellite lines were eliminated by use of a multiple technique using an analytical computer system. Peak areas were calculated through a normalization procedure which accounted for the acquisition time and a data point step of 0.05 eV. Depth analysis was performed by etching the surface with a current density of 10 $\mu A\,cm^{-2}$ and a 5 keV $Ar^+$ ion beam. The sputtering rate was estimated to be about 0.1 nm $\mu A^{-1}\,min^{-1}\,cm^2$.

### 2.5. TEM and SEM observation

TEM observation was performed in a JEM-100 CX Electron Microscope. After TEM observation the same grid or glass grids were coated with a thin layer of gold then mounted in an SEM (Hitachi X-650).

### 2.6. X-ray microprobe analysis

The selected area of the sample was analysed with an EDAX 9100 energy-dispersion type X-ray analyser attached to a TEM. Elemental iron, phosphorus and chlorine were determined from the X-ray intensity of $FeK_a$, $PK_a$ and $ClK_a$ line emission. Quantitive calculation was made.

### 2.7. Differential scanning calorimetry (DSC)

DSC measurement was performed in pure argon gas with a heating rate of 20 K $min^{-1}$.

### 2.8. Inductively coupled plasma (ICP) analysis

The content of iron and phosphorus was analysed by an inductively coupled plasma method (ICP) with an Atomscan 200 ICP-AES instrument.

### 2.9. X-ray diffraction (XRD)

XRD measurement was performed using $CuK_a$ X-ray radiation with a monochromator mounted on the diffracted beam.

## 3. Results and discussion

### 3.1. The formation and morphology of iron and phosphorus particles

Fig. 2 shows the iron particle (sample PL1) which is basically spherical with a diameter of 10–100 nm. The particle size is a little different at different positions. Selected-area electron diffraction shows that the particle is microcrystalline. When $PCl_3$ was treated with argon plasma, ultrafine amorphous phosphorus particles were formed. Fig. 3a and b show transmission electron micrographs of the phosphorus particles in positions A and B respectively. Most of the particles are irregular in shape with a size of 2–40 nm and very well dispersed. Fig. 3c shows a scanning electron micrograph of PL2a. Sample PL2b is similar to PL2a

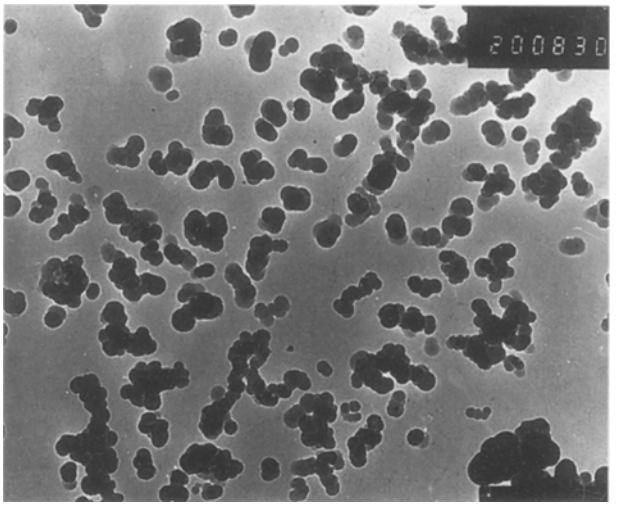

*Figure 2* Transmission electron micrograph selected-area electron diffraction image of sample PL1.

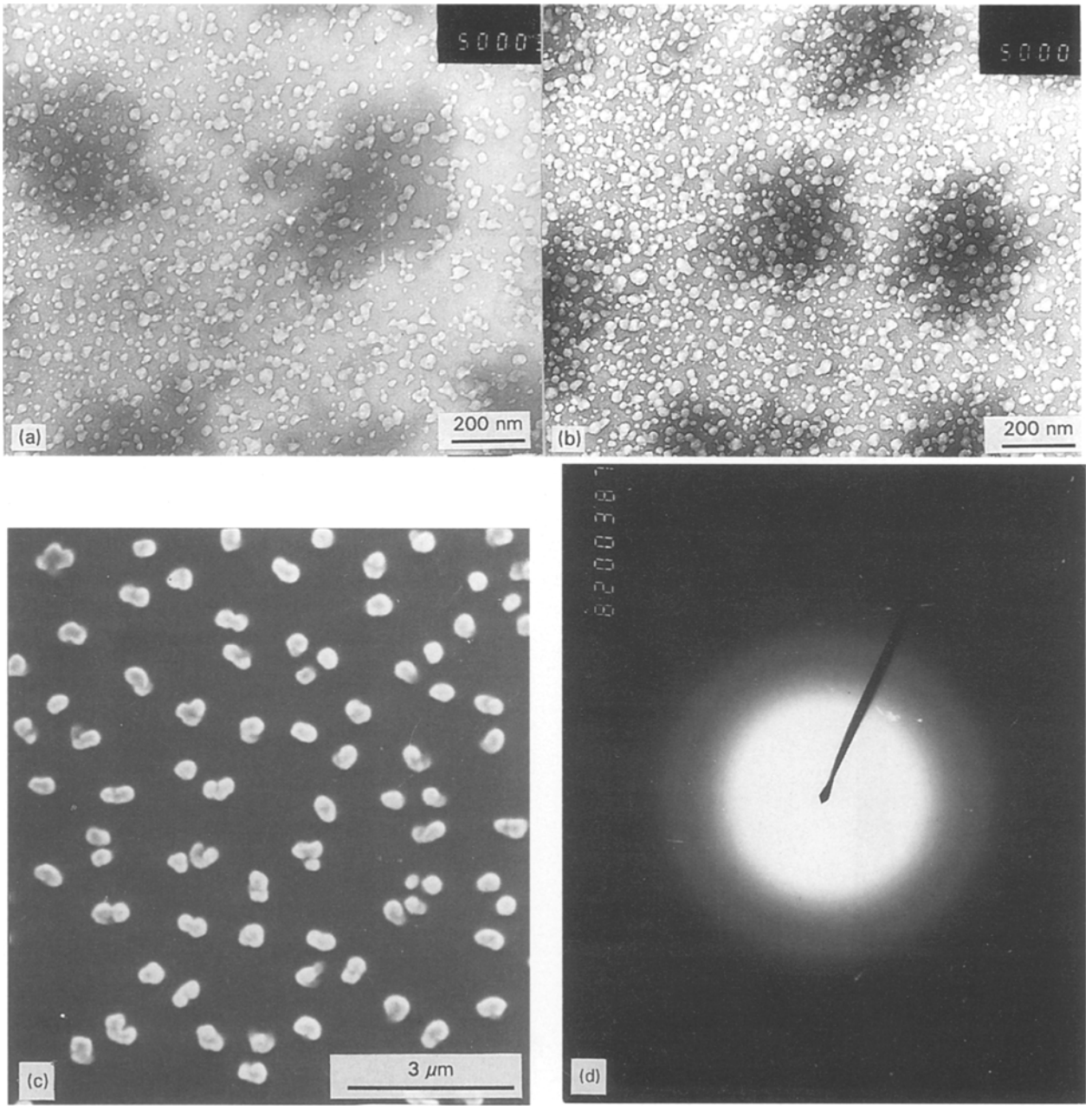


*Figure 3* Transmission electron micrographs at (a) position A, (b) position B, (c) scanning electron micrograph, and (d) selected-area electron diffraction image of sample PL2a.

The particle is in an amorphous state, as indicated by the selected-area electron diffraction image (Fig. 3d). X-ray surface microprobe analysis indicates that there elemental chlorine exists in the ultrafine phosphorus (Fig. 4a), but virtually no chlorine was found in samples PL2b produced under hydrogen plasma (Fig. 4b). This is because chlorine can react with hydrogen to form HCl which can be evacuated by pumping.

## 3.2. The formation and composition of Fe–P alloy particles

It is very interesting to find that neither phosphorus nor microcrystalline iron particles, but amorphous Fe–P alloy was formed when $PCl_3$ and $Fe(CP)_2$ were mixed under plasma conditions. Transmission electron micrographs show that the particles are roughly spherical and have a diameter of about 40–200 nm (Fig. 5). Fig. 5c shows a scanning electron micrograph of the sample. Fig. 5d is the selected-area electron diffraction pattern, indicating the amorphous status of the particles; this was also confirmed by the X-ray diffraction profile in which only a very broad peak in the vicinity of about 45 was determined. X-ray microprobe analysis gave not only the $FeK_a$ and $PK_a$ lines emission but also the $ClK_a$ line emission. The composition of the Fe–P particles in different positions was not entirely the same. The analytical results of different regions in different positions (A and B) are listed in Table II. Typical surface analysis is shown in Fig. 6. From Table II, the mole ratio of Fe/P in different positions (A and B) is almost the same (2.02 for position A and 1.96 for position B) although the content of iron and phosphorus in position A is a little

higher than that in position B. However the chlorine content is lower than the latter, indicating that the amorphous Fe–P alloy is in the composition of $Fe_2P$. This basically agrees with ICP result (Fe: 54.6 and P: 13.8 at wt%, mole ratio of Fe/P = 2.12). As shown in Fig. 4a, chlorine also exists in amorphous phosphorus (PL2). So, the two different states of chlorine may be phosphorus-bounded and carbon-bounded chlorine in sample PL3. This is also proved by the infrared spectra and XPS spectra.

The formation of the Fe–P amorphous particles was also characterized by infrared spectroscopy. Fig. 7 shows the IR spectra of $Fe(Cp)_2$ and plasma-treated deposition products. It is found that the absorption at 475.3 $cm^{-1}$ which is the $\gamma$(M-R) stretching vibration of the Fe-(cyclopendienyl) group disappeared in sample PL3, indicating the decomposition of $Fe(Cp)_2$ structure. Several new absorptions at 1642.2, 1611.2 $cm^{-1}$ which are $\gamma$(C=C) absorption and 3104.1, 2953.3 and 2866.4 $cm^{-1}$ which are $\gamma$(C–H) absorption appeared. This indicates the formation of a carbon-hydrogen compound containing saturated alkyl and unsaturated alkenyl chains. This is also confirmed by the ICP result which gives 56.3% iron by weight in the product. The absorptions at 493.5 and 852.8 $cm^{-1}$ are attributed to P–Cl and C–Cl stretching vibrations. The existence of chlorine in sample PL3 is also proved by selected-area X-ray microprobe analysis (Fig. 6). The absorption at 1701.1 and 3400.3 $cm^{-1}$ in sample PL3 is due to further reaction of the trapped radical with oxygen, and the oxidation of surface iron particles, and also water after the sample was exposed to air. From Fig. 7, very strong absorptions at 1002.7 and 1148.8 $cm^{-1}$, which

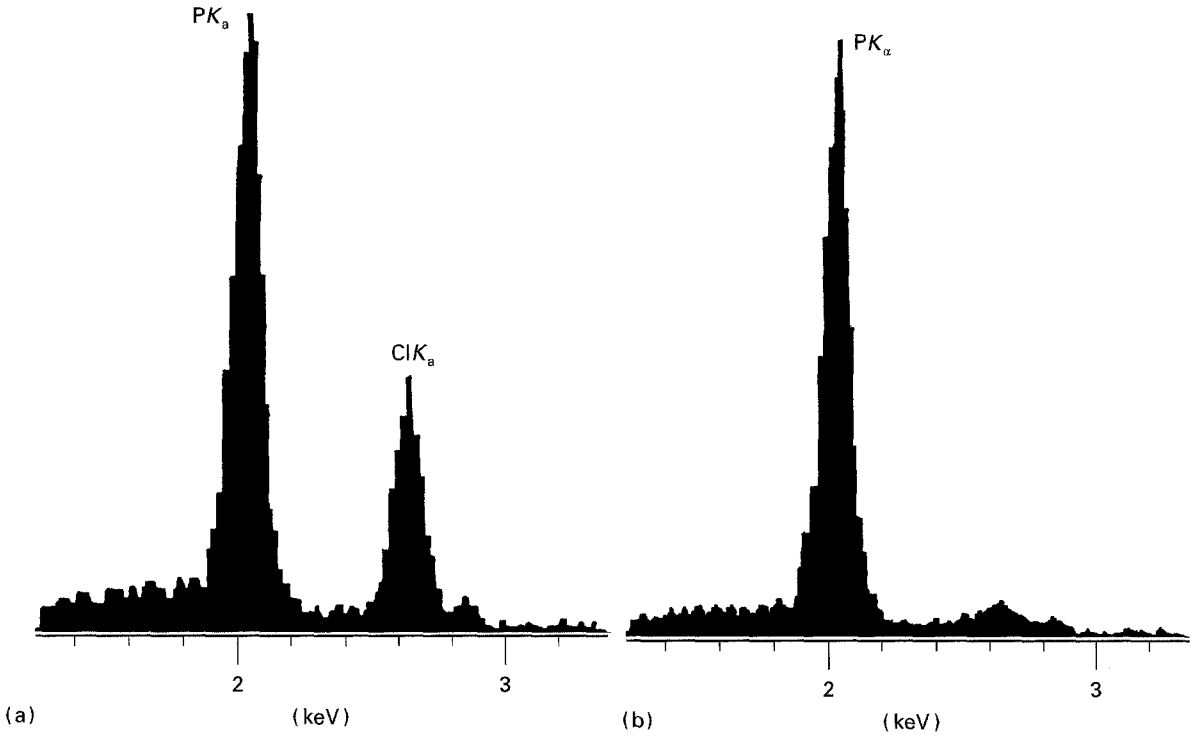


*Figure 4* X-ray microprobe analysis of samples (a) PL2a and (b) PL2b.

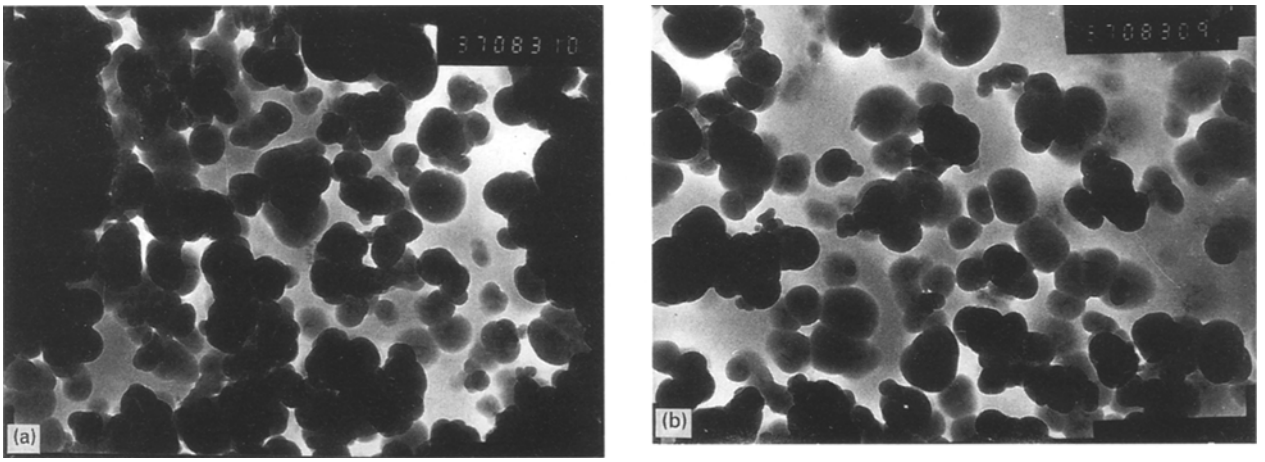


*Figure 5* Transmission electron micrographs at (a) position A, and (b) position B, (c) scanning electron micrograph, and (d) selected area electron diffraction image, of sample PL3.

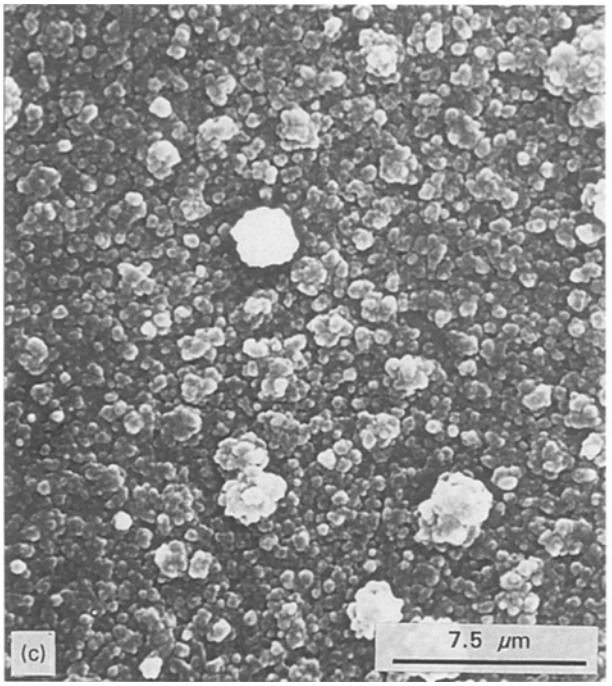


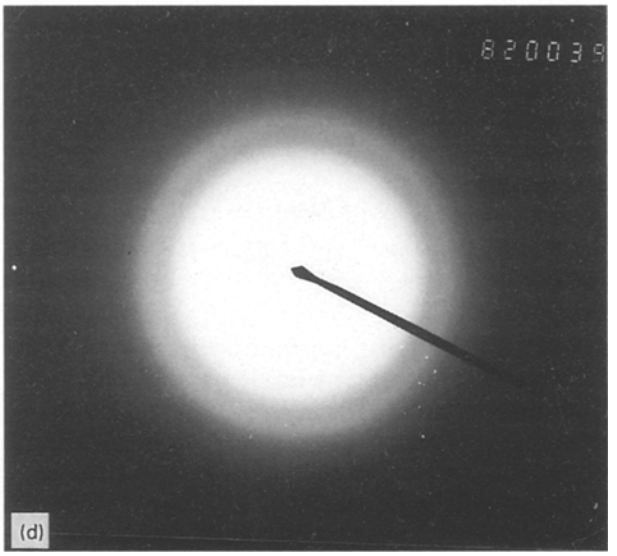


*Figure 5* (Continued).

TABLE II Composition of Fe–P particles by X-ray microprobe analysis

| Position | Region | Element | Fit index | (wt%) | Mole ratio | Average mole ratio |
|---|---|---|---|---|---|---|
| A | I | P | 0.60 | 13.4 | 43.1 | Fe: 88.3 |
| | | Cl | | 37.7 | 10.6 | P: 43.8 |
| | | Fe | | 48.9 | 87.6 | Cl: 10.6 |
| | II | P | 0.64 | 13.8 | 44.5 | Fe/P = 2.02 |
| | | Cl | | 37.4 | 10.5 | |
| | | Fe | | 49.8 | 88.9 | |
| B | I | P | 0.68 | 13.0 | 41.8 | Fe: 79.1 |
| | | Cl | | 43.4 | 12.2 | P: 40.3 |
| | | Fe | | 43.6 | 78.1 | Cl: 12.2 |
| | II | P | 0.65 | 12.0 | 38.8 | Fe/P = 1.96 |
| | | Cl | | 43.1 | 12.1 | |
| | | Fe | | 44.9 | 80.1 | |

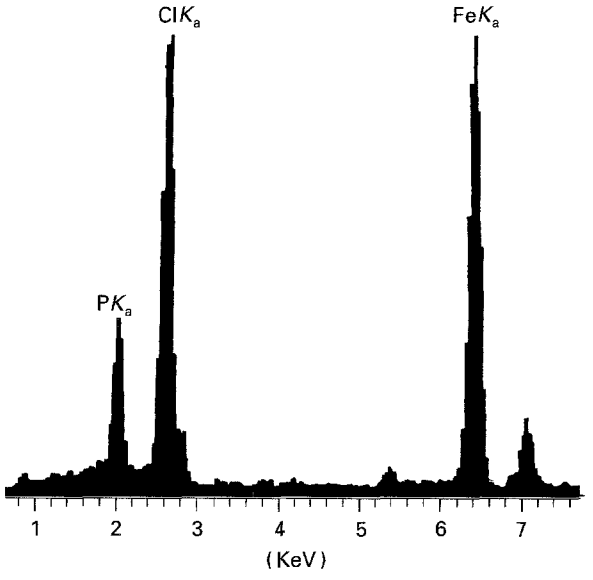


*Figure 6* Typical X-ray microprobe analysis of sample PL3.

are P–OH and P=O stretching vibrations, can be determined in sample PL2a, which indicated that the amorphous phosphorus is easily oxidized. However, compared with sample PL2a, samples PL3 and PL4 do not exhibit these absorptions. This implies that the stability of phosphorus in air increases when it becomes an amorphous alloy with iron.

Based on the experimental results above, the Fe-(cyclopendienyl) group was decomposed to form activated iron atoms and carbon-hydrogen species such as C, $CH_x$($x = 1, 2$ or 3) and CH=CH, etc. $PCl_3$ was also decomposed to form atomic phosphorus $PCl_x$- and Cl-activated species (those active species include dissociated atoms, ions, radicals, activated atoms or molecules). Iron and phosphorus atoms reacted in the gas and aggregated to form ultrafine amorphous Fe–P alloy particles. Carbon-hydrogen species also reacted to form carbon-hydrogen compounds and were deposited. The mechanism of the formation of ultrafine Fe–P amorphous particles can be described as

follows

$$Fe(CP)_2 \rightarrow Fe(atom) + 2Cp \quad (1)$$

$$PCl_3 \rightarrow PCl_x(x = 1, 2) + P + nCl \quad (2)$$

$$Cp \rightarrow (C, CH, CH_2\ CH{=}CH \text{ etc.}) \xrightarrow[\text{and deposition}]{\text{polymerization}} \quad (3)$$

$$nFe + nP \rightarrow Fe\text{–}P \text{ alloy particle} \quad (4)$$

$$Cl + H \rightarrow HCl \quad (5)$$

$$Cl + C_xH_y \rightarrow Cl\text{–}C_xH_y \quad (6)$$

## 3.3. Influence of plasma condition on the formation of Fe–P particles

Plasma gas greatly influences not only the morphology but also the composition of the Fe–P particles. Compared with sample PL3, the Fe–P particles (sample PL4) are smaller and more uniform (Fig. 8).

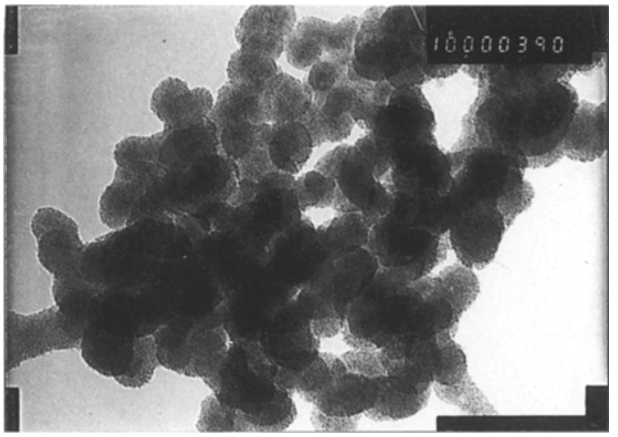

*Figure 8* Transmission electron micrographs of sample PL4.

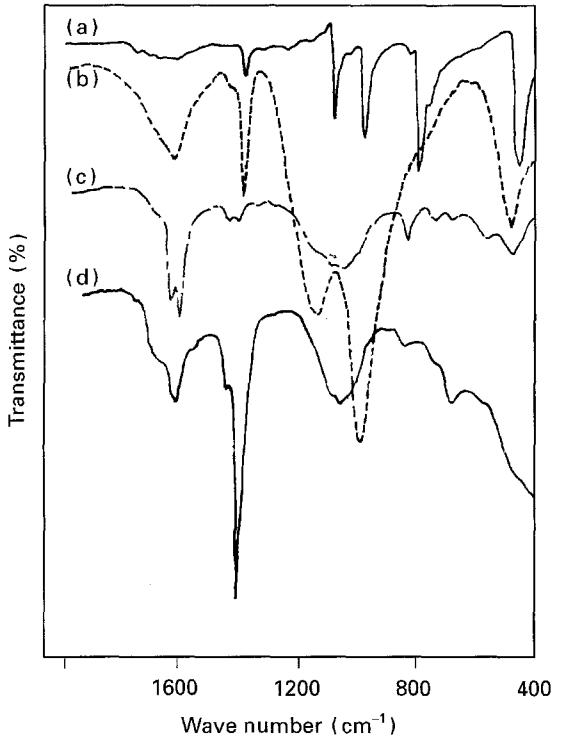


*Figure 7* FT–IR spectra of (a) $Fe(CP)_2$, (b) PL2a, (c) PL3, and (d) PL4.

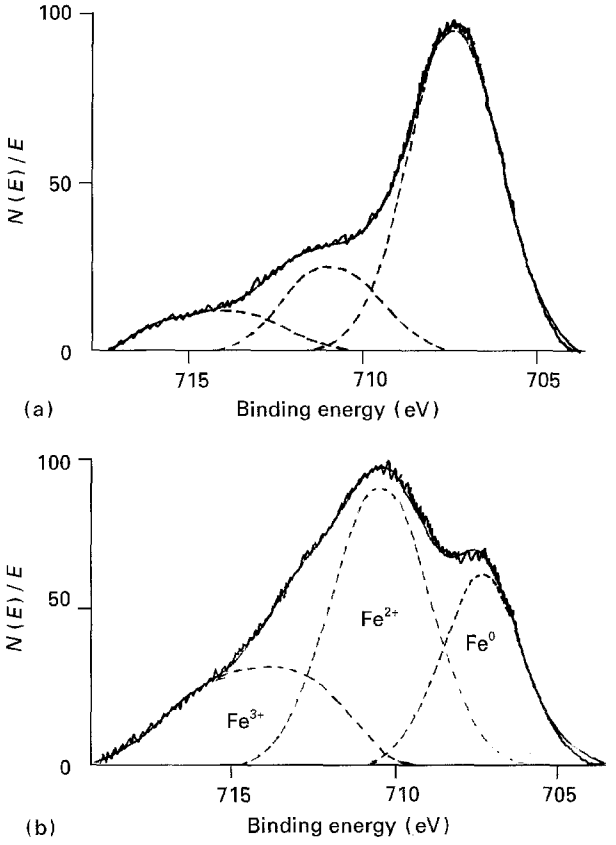


*Figure 9* XPS spectra of $Fe2P_{3/2}$ of sample PL4: (a) exposed to air for less than 5 min, (b) exposed to air for 24 h.

TABLE III Infrared frequencies and band assignment

| Frequency assignment ($Fe(CP)_2$) ($cm^{-1}$) | Frequency assignment (PL2a) ($cm^{-1}$) | Frequency assignment (PL3) ($cm^{-1}$) | Frequency assignment (PL4) ($cm^{-1}$) |
|---|---|---|---|
| 475.3 γ(M–R) | 1002.7 γ(P–OH) | 1642.2 γ(C=C) | 1618.8 γ(C=C) |
| 816.1 | 1148.8 (γ(P = O) | 1611.2 | 1673.9 |
| 852.5 π(C–H) | 496.4 γ(P–Cl) | 1401.2 δ($CH_2$) | 1400.1 δ($CH_2$) |
| 1000.4 δ(C–H) | 1400.7 (?) | 493.5 γ(P–Cl) | 689.7 (?) |
| 1104.2 γ(C = C) | 1636.6 (?) | 852.8 γ(C–Cl) | 851.0 γ(C–Cl) |
| 1406.4 δ($CH_2$) | | 1062.7 γ(C–O) | 1065.1 γ(C–O) |
| 3089.4 γ(C–H) | | 1701.1 γ(C=O) | 3200.7 γ(C–H) |
| | | 3104.1 γ(C–H) | 3124.4 |
| | | 2953.3 | 2960.8 |
| | | 2866.4 | |

TABLE IV Surface composition (at %) and binding energy data of the particles

| Sample | Fe | P | O | C | Cl | $Fe2P_{3/2}$ (eV) | States and ratio | $P_{2P}$ (eV) | States and ratio | $Cl_{2P}$ (eV) |
|---|---|---|---|---|---|---|---|---|---|---|
| PL2a | – | 30.9 | 19.1 | 37.2 | 12.8 | – | – | 130.1 | $P^0$(90.2%) | 198.9 |
| | | | | | | | | 133.8 | $p^{n+}$(9.8%) | |
| PL2b | | 39.8 | 20.4 | 38.8 | | – | – | 129.9 | $P^0$(91.7%) | – |
| | | | | | | | | 133.2 | $p^{n+}$(8.3%) | |
| PL2b[a] | – | 25.3 | 38.1 | 36.6 | – | – | – | 130.0 | $P^0$(21.5%) | – |
| | | | | | | | | 133.4 | $p^{n+}$(78.5) | |
| | | | | | | 707.3 | $Fe^0$(82.2%) | 130.3 | $P^0$(92.4%) | |
| PL3 | 3.8 | 3.6 | 9.9 | 74.2 | 8.5 | 710.1 | $Fe^{2+}$(9.2%) | 133.3 | $p^{n+}$(7.6%) | 198.7 |
| | | | | | | 713.9 | $Fe^{3+}$(8.6%) | | | |
| | | | | | | 707.2 | $Fe^0$(81.0%) | 130.2 | $p^0$(94%) | |
| PL4 | 6.2 | 5.8 | 12.6 | 69.6 | 5.8 | 710.4 | $Fe^{2+}$(12.2%) | 133.3 | $p^{n+}$(6%) | 198.8 |
| | | | | | | 714.0 | $Fe^{3+}$(7.8%) | | | |
| | | | | | | 707.3 | $Fe^0$(23.1%) | 130.2 | $p^0$(36.4%) | |
| PL4[a] | 5.9 | 5.6 | 18.2 | 64.7 | 5.6 | 710.5 | $Fe^{2+}$(55.4%) | 133.4 | $p^{n+}$(63.6%) | 198.8 |
| | | | | | | 714.0 | $Fe^{3+}$(21.5%) | | | |

[a] Sample was exposed to air for 24 h at room temperature.

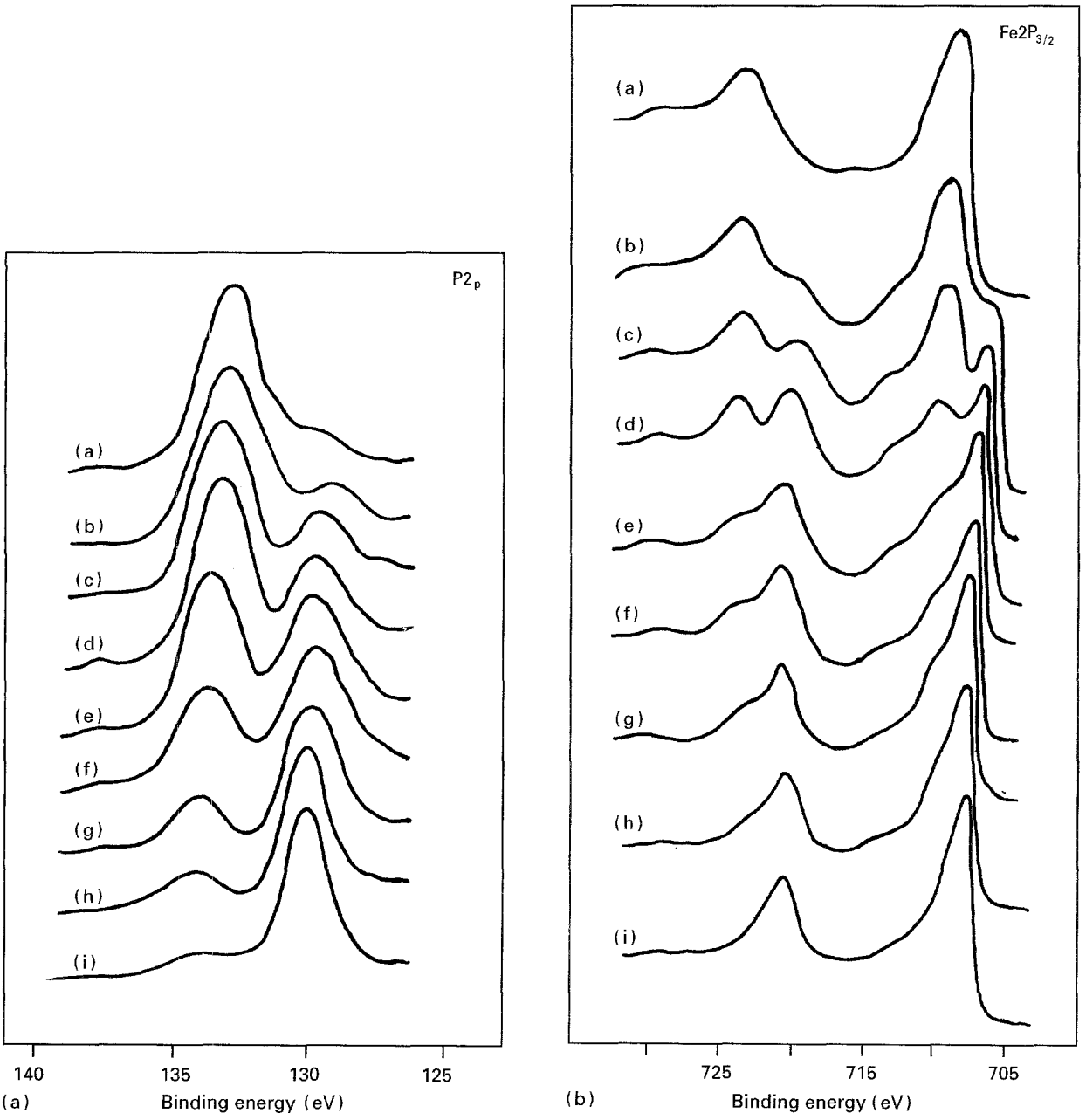


*Figure 10* Fe2p and P2p XPS spectra of PL4 as a function of sputter time: surfaces exposed to air for (a) 1 week, (b) 5 min, (c) 10 min, (d) 15 min, (e) 20 min (f) 25 min, (g) 30 min, (h) 35 min, and (i) 40 min.

X-ray microprobe analysis shows that the chlorine content in sample PL4 is less than in PL3. This agrees with the PL2a and PL2b situation (discussed above). XPS quantitative calculation gives the surface composition of the particle surface (Table III). Fig 9a and b are $Fe2P_{3/2}$ XPS spectra of sample PL4 showing its original surface and the surface after exposure to air for 24 h.

From Table III, no distinct $Cl_{2P}$ was determined in sample PL2 deposited under a hydrogen plasma, which agrees with the results of X-ray microprobe analysis. However, chlorine was still determined in sample PL4, although it was deposited under a hydrogen plasma. However, the chlorine content is less than that in sample PL3. This is because some chlorine atoms are bounded with carbon and are deposited. IR spectra also show the C–Cl stretching vibration absorption (Table III). It was noted that there was no absorption at 493 $cm^{-1}$ which is the P–Cl stretching vibration, and just a weak absorption at 851 $cm^{-1}$ can

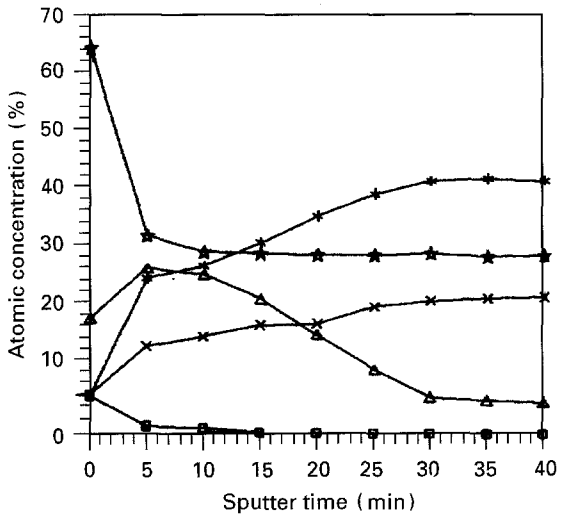


*Figure 11* Changes in elemental abundance in the surface as a function of sputtering time (sample PL4). (*) Fe, (×) P, (☆) C, (△) O, (□) Cl.

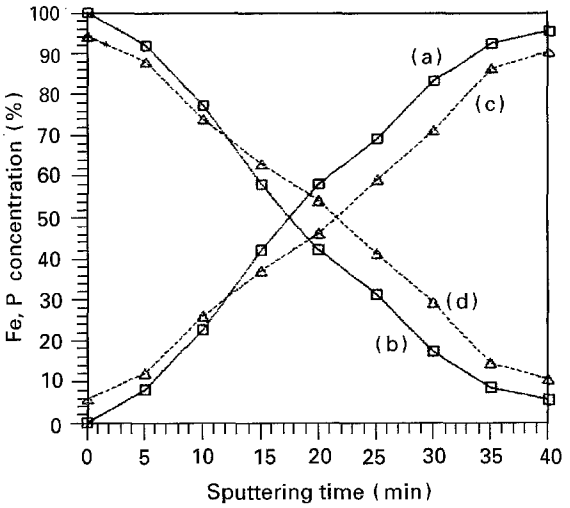


*Figure 12* Relative quantitivity of different states of iron and phosphorus as a function of sputtering time: (a) $Fe^0/Fe_{total}$, (b) $Fe_{oxidized}/Fe_{total}$, (c) $p^0/P_{total}$, (d) $P_{oxidized}/P_{total}$.

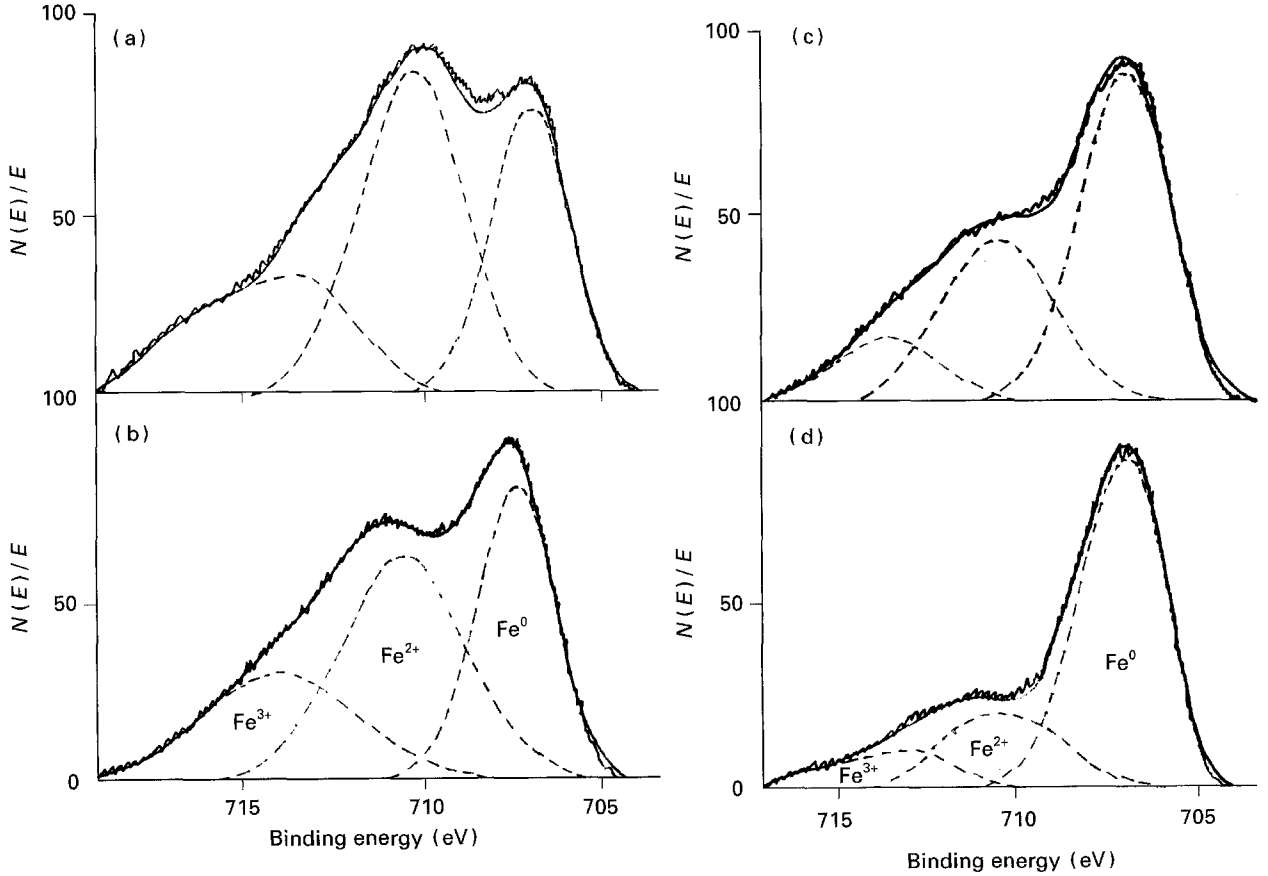


*Figure 13* Some typical XPS spectra of $Fe2P_{3/2}$ of sample PL4 after sputtering times (a) 5 min, (b) 15 min (c) 25 min, and (d) 35 min.

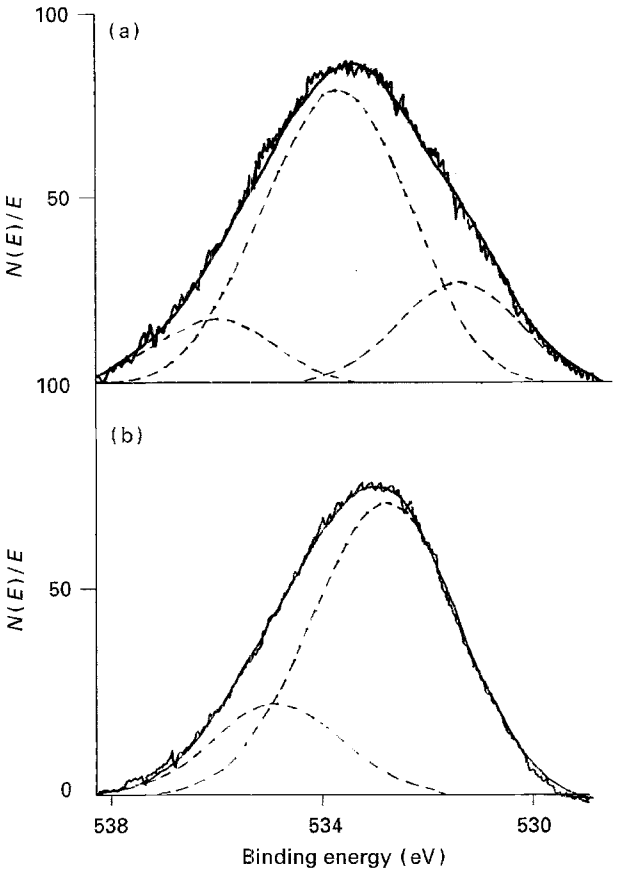


*Figure 14* $O_{1s}$ XPS spectra of sample PL4 after (a) no sputtering, and (b) sputtering for 25 min.

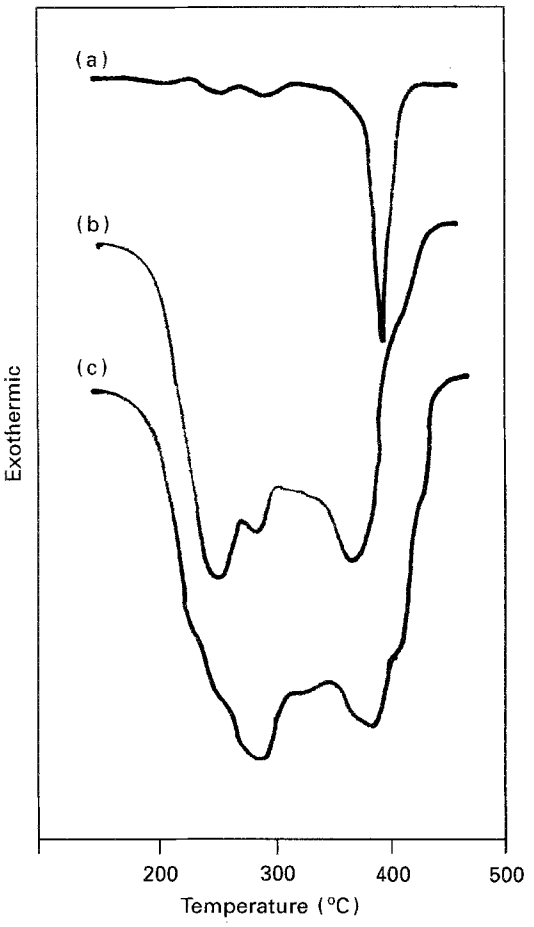


*Figure 15* Differential scanning calorimetry profile of (a) sample PL2b, (b) sample PL3 and (c) sample PL4.

be seen in sample PL4. This implies that the chlorine content in sample PL4 is much less than that of PL3 and the chlorine was mainly bounded to carbon. From Table IV the relative quantity of oxidized phosphorus in the surface of sample PL4* (63.6%) is seen to be less than that in sample PL2b* (78.5%) when exposed to air for 24 h, suggesting the formation of iron and phosphorus alloy improves the stability of phosphorus in air. Therefore, more uniform Fe–P alloy particles with less chloride were formed under a hydrogen plasma condition.

## 3.4. The surface states and the stability of the iron particles

XPS spectra have indicated that part of the iron on the surface of sample PL4 was oxidized, even if the sample was exposed to air for less than 5 min (Fig. 9a). Oxidized iron, which is a complex of $Fe^{2+}$ and $Fe^{3+}$, decreased when sample PL4 was exposed to air for 24 h (Fig. 9b), and some of the phosphorus was also oxidized. All the iron in the particle surface became oxidized states after exposure to air for 1 week at room temperature (Fig. 10). The sputtering experiment shows that the zero valence iron increases with increasing sputtering depth (Fig. 11). According to the estimation of the etching rate of 0.1 nm $\mu A^{-1}$ $min^{-1}$ $cm^{-2}$, the oxidation layer is about 30 nm deep. A similar situation is found for elemental phosphorus (Fig. 10). Fig. 12 shows the relative quantity of different states of iron and phosphorus as a function of sputtering time. From Fig. 10, the Fe/P atomic ratio is seen to decrease with sputtering time, implying phosphorus enrichment in the particle surface. After 5 min sputtering, the carbon content remains constant and the chloride content was almost non-determinable. Some typical $Fe2P_{3/2}$ XPS pictures are shown in Fig. 13. The differences between the surface and the inside of the sample can also be seen from $O_{1s}$ XPS spectra (Fig. 14). Fig. 14a shows the original surface (no sputtering) where three kinds of oxygen exist. Fig. 14b shows the internal surface after sputtering for 25 min where only two kinds of oxygen appear.

The crystallization properties of the Fe–P amorphous alloy particles were studied by differential scanning calorimetry. As shown in Fig. 15, the crystallization temperature of amorphous phosphorus (sample PL2b) is at 410 °C. Two main peaks at 250 and 382 °C were found in a sample of Fe–P amorphous particles (PL3) and at 287 and 384 °C in sample PL4. No distinct peak appeared at 410 °C. This indicates phosphorus in samples PL3 and PL4 is in the alloying states.

## 4. Conclusions

1. Ultrafine amorphous Fe–P alloy particles can be directly synthesized by the plasma method using cyclopentenyl iron phosphorus trichloride as starting materials. The particles are roughly spherical with a diameter of 40–200 nm and have the composition of

$Fe_2P$. About 25–35 wt% is carbonhydrogen compounds in the powders.

2. The plasma gas greatly influences the morphology, dispersion and composition. Elemental chlorine was found in the surface of the particles, especially when prepared under argon plasma conditions. It was bonded to phosphorus and carbon in Fe–P particles prepared with an argon plasma and bonded mainly to carbon in Fe–P particles deposited under a hydrogen plasma.

3. The formation of Fe–P increases the stability of phosphorus in air, and phosphorus is relatively enriched in the surface of Fe–P amorphous particles.

## References


1. H. S. CHEN, *Rep. Prog. Phys.* **43** (1980) 353.
2. G. HERZER and H. R. HILZINGER, in "Magnetic Properties of Amorphous Metals" (Elsevier, 1987) p. 354.
3. A. INOU, J. SAIDA, and T. MASUMOTO *Metall. Trans.* **19A** (1988) 2315.
4. S. LINDEROTH, S. MORUP and M. D. BENTZON, *J. Magn. Magn. Mater.* **83** (1990) 457.
5. F. E. LUBORSKY (ed.), "Amorphous Metallic Alloys" (Butterworth, 1983).
6. R. L. ZELLER III and U. LANDAU, *J. Electrochem. Soc.* **138** (1991) 1010.
7. K. SUMIYAMA and Y. NAKAMURA, *Trans. Jpn Inst. Metals* **29** (1983) 283.
8. T. SAWADA, C. S. PAI and S. S. LAU, *J. Mater. Res.* **1**(2) (1986) 322.
9. E. MA, B. X. LU and H. D. LI, in "MRS Conference" Boston (1985).
10. M. NATAN, *Appl. Phys. Lett.* **48** (1986) 707.
11. N. BURGIO, G. ENNAS, M. MAGINI, F. PADELLA, B. SCHIPPA and P. SUSINI, "Solid State Powder Procesing", edited by A. H. Clauer and J. J. de Barbadillo (Mineral, Metals and Materials Society, 1990), p. 344.
12. A. CORRIAS, G. ENNAS, G. MARONGIU and G. PASCHINA, *J. Mater. Soc.* **26** (1991) 5081.
13. R. A. BRAND, J. LAUER and D. HERLACH, *J. Phys. F.* **13** (1983) 675.
14. J. WONTERGHEM, S. MORUP, C. J. W. KOCH, S. W. CHARLES and S. WELLS, *Nature* **322** (1986) 622.
15. A. CORRIAS, S. G. ENNAS, G. LICHERI, G. MARONGIU and G. PASCHINA, *Chem. Mater.* **2** (1990) 363.
16. J. P. GONG, Y. KAGAMI, K. YAMADA and Y. OSADA, *Bull. Chem. Soc. Jpn* **63** (1990) 1578.
17. E. KAY and M. HECQ, *J. Appl. Phys.* **55** (1984) 370.
18. K. AKASHI, "Progress in Thermal Plasma Deposition of Alloys and Ceramics Fine Particles" ISPC-7, Eindhoven, 1985, p. 13.
19. T. N. MEYER, A. J. BECKER, J. E. EDD, F. N. SMITH and J. JIU, "Plasma Synthesis of Ceramics Powders ISPC-8, Tokyo, 1987, p. 2006.
20. C. W. ZHU, G. Y. ZHAO, V. V. S. REVANKAR and V. HLAVACEK, *J. Mater. Sci.* **27** (1992) 2211.
21. K. ISHIZAKI, T. EGASHIRA, K. TANAKA and P. B. CELIS, *Ibid.* **24** (1989) 3552.



*Received 8 November 1993*
*and accepted 10 October 1994*